THE JOURNAL OF PHYSICAL CHEMISTRY LETTERS
A JOURNAL OF THE AMERICAN CHEMICAL SOCIETY

pubs.acs.org/JPCL

Letter

Phonon-Mediated Exciton Relaxation in Two-Dimensional Semiconductors: Selection Rules and Relaxation Pathways

Xiao-Wei Zhang, Kaichen Xie, En-Ge Wang,* Xin-Zheng Li,* and Ting Cao*

Cite This: *J. Phys. Chem. Lett.* 2024, 15, 7584−7590

Read Online

ACCESS | Metrics & More | Article Recommendations | Supporting Information

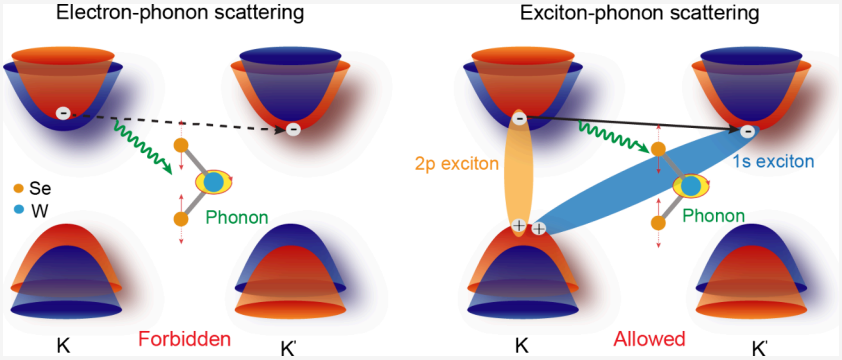

ABSTRACT: Exciton−phonon coupling (ExPC) is crucial for energy relaxation in semiconductors, yet the first-principles calculation of such coupling remains challenging, especially for two-dimensional (2D) systems. Here, an accurate method for calculating ExPC is developed and applied in exciton relaxation problems in monolayer WSe_2. Considering the interplay between the exciton wave functions and electron−phonon coupling (EPC) matrix elements, we find that ExPC shows selection rules distinct from the ones of EPC. By employing the Wannier exciton model, we generalize these selection rules, which state that the angular quantum numbers of the exciton must match the winding numbers of the EPC matrix elements for the ExPC to be allowed. To verify our theory and method, we calculate intervalley exciton relaxation pathways, which agree well with a recent experiment.

Phonons and their interactions with electronic quasiparticles play critical roles in the optical properties and relaxation dynamics of materials. In conventional semiconductors such as GaAs, hot carrier thermalization has been mostly studied in the context of EPC.[1,2] In recent years, 2D materials have emerged as a fertile platform for studies of novel optical properties absent in bulk systems.[3−8] The reduced dielectric screening and quantum confinement effects induce a fraction of eV exciton binding energies in 2D semiconductors like monolayer transition metal dichalcogenides (TMD).[6,9] As a result, optical excitation can directly create sub-bandgap and tightly bound excitons. Phonon-mediated scattering between different excitonic states therefore becomes ubiquitous in their energy relaxation dynamics, exciton recombination, and photoluminescence processes.[9] Several first-principles approaches have been developed to address such exciton−phonon coupling (ExPC) problems, including many-body perturbation theory,[10−13] nonadiabatic molecular dynamics,[14,15] time-dependent density functional theory,[16] and the density matrix approach.[17] Despite these advancements, accurately and efficiently calculating ExPC remains a challenge.[10−21] Furthermore, whether ExPC exhibits fundamentally different physical behaviors from EPC in these 2D systems remains an open question.

In this article, we investigate phonon-mediated exciton relaxation in 2D semiconductors, by directly analyzing ExPC instead of EPC. This is enabled by a newly developed method for calculating ExPC. Monolayer WSe_2 is chosen as an example due to its large excitonic effects and the emergence of multiple nearly degenerate valleys.[22−26] We show that ExPC can result in distinct selection rules compared with the analysis of EPC. The interplay between the exciton envelope functions on a two-particle basis and the EPC matrix elements plays a crucial role. Using the 2D Wannier exciton model, we provide a simple picture for the rationalization of these rules, where the change of exciton angular quantum numbers is compensated by the winding number of EPC matrix elements. To verify our theory and method, we calculate the intervalley exciton−phonon scattering times, which agrees well with a recent experiment.[26]

Received: May 16, 2024
Revised: July 9, 2024
Accepted: July 12, 2024
Published: July 18, 2024

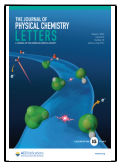

Downloaded from pubs.acs.org/jpclcd/article-pdf/15/30/7584/3367608/jz4c01433.pdf by PEKING UNIV user on 04 November 2026

© 2024 American Chemical Society

https://doi.org/10.1021/acs.jpclett.4c01433
J. Phys. Chem. Lett. 2024, 15, 7584−7590

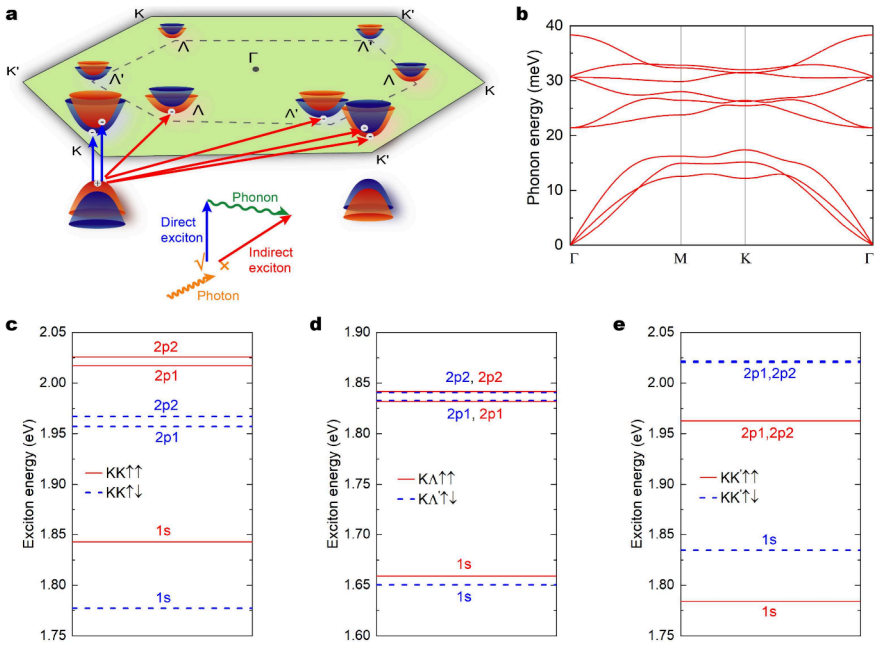

Figure 1. Excitons, phonons, and schematic exciton−phonon interactions in monolayer WSe_2. (a) The first BZ of monolayer WSe_2. The orange and blue parabolas denote the spin-up and spin-down bands, respectively. Inside the first BZ, there are three Λ points, three Λ′ points, one K point and one K′ point. Bottom: the schematic diagram of exciton−phonon scattering. A photon (orange wavy arrow) can create direct excitons (blue arrow) but cannot create indirect excitons (red arrow) due to momentum mismatch. Phonon (green wavy arrow) can scatter direct excitons to indirect excitons by contributing a finite momentum. (b) Phonon dispersion along high-symmetry lines. (c−e) Eigenvalues of KK (c), KΛ (d), and KΛ′ (d), and KK′ (e) excitons, including 1*s* and 2*p*, like-spin (solid red lines) and unlike-spin (dashed blue lines) states.

The Hamiltonian of the exciton−phonon coupled system reads[27,28]

$$H = \sum_{S\mathbf{Q}} \Omega_{S\mathbf{Q}} a^{\dagger}_{S\mathbf{Q}} a_{S\mathbf{Q}} + \sum_{\mathbf{q}\nu} \left(b^{\dagger}_{\mathbf{q}\nu} b_{\mathbf{q}\nu} + \frac{1}{2}\right)\hbar\omega_{\mathbf{q}\nu} + \sum_{SS'\mathbf{Q}\mathbf{q}\nu} G_{S'S}(\mathbf{Q}, \mathbf{q}\nu) a^{\dagger}_{S'\mathbf{Q}+\mathbf{q}} a_{S\mathbf{Q}} (b_{\mathbf{q}\nu} + b^{\dagger}_{-\mathbf{q}\nu}) \quad (1)$$

Here, the first term treats excitons as noninteracting bosons using exciton creation and annihilation operators, $a^{\dagger}_{S\mathbf{Q}}$ and $a_{S\mathbf{Q}}$. $\Omega_{S\mathbf{Q}}$ is the exciton eigenvalue with the center-of-mass momentum $\mathbf{Q}$ and band index S. $\Omega_{S\mathbf{Q}}$ can be solved from the Bethe-Salpeter equation (BSE).[29,30] The eigenfunction of the BSE gives the exciton wave function, $\chi^{\mathbf{Q}}_{S}(\mathbf{r}_e, \mathbf{r}_h) = \sum_{vck} A^{S}_{vk,ck+Q} \psi_{ck+Q}(\mathbf{r}_e) \phi^{*}_{vk}(\mathbf{r}_h)$. The exciton wave function consists of an envelope function $A^{S}_{vk,ck+Q}$ that carries the angular momentum of the exciton, and the Bloch wave function of the electron (hole) ψ_{ck+Q} (ϕ_{vk}). The second term of eq 1 represents the noninteracting phonon system, where $b_{q\nu}$ ($b^{\dagger}_{q\nu}$) is the phonon annihilation (creation) operator and $\omega_{q\nu}$ is the frequency. The third term of eq 1 is the first-order ExPC Hamiltonian and the ExPC matrix element is defined as[28]

$$G_{S'S}(\mathbf{Q}, \mathbf{q}\nu) = \sum_{\mathbf{k}vcc'} A^{S'*}_{vk,c'k+Q+q} A^{S}_{vk,ck+Q} g_{c'c}(\mathbf{k} + \mathbf{Q}, \mathbf{q}\nu) - \sum_{\mathbf{k}cvv'} A^{S'*}_{vk-q,ck+Q} A^{S}_{v'k,ck+Q} g_{v'v}(\mathbf{k} - \mathbf{q}, \mathbf{q}\nu) \quad (2)$$

where $g_{mn}(\mathbf{k}, \mathbf{q}\nu) = \langle m\mathbf{k} + \mathbf{q}|\delta_{q\nu} V^{\mathrm{scf}}|n\mathbf{k}\rangle$ is the EPC matrix element. Equation 2 defines the relationship between the ExPC and EPC matrix elements, G and g, and serves as the starting point of our analyses. The minus sign ahead of the second term of eq 2 arises from the energy difference between the electron and hole, which contributes to the exciton energy.

First-principles calculations of the ExPC matrix elements G in eq 2 are numerically intensive and challenging. First, accurate descriptions of the exciton envelope function of the BSE require very dense Brillouin zone (BZ)-sampling, especially in 2D semiconductors.[31,32] Second, finite-momentum excitons involved in the exciton−phonon problems further increase the complexity of the problem. Third, the gauge degree of freedom in the calculations of the exciton envelope function and the EPC matrix elements often causes a phase mismatch between the two. Owing to these difficulties, accurate first-principles calculations of ExPC matrix elements and scattering times for noncentrosymmetric monolayer semiconductors remain challenging.

We calculate the exciton envelope functions and EPC matrix elements in eq 2 by first-principles GW-BSE method implemented in BerkeleyGW[30,33] and density-functional perturbation theory (DFPT) implemented in Quantum ESPRESSO.[34] Although the ExPC matrix element G is gauge-invariant (up to a trivial phase), the exciton envelope functions and EPC matrix elements in eq 2 can carry arbitrary gauges and introduce numerical difficulties in first-principles calculations as well as the interpretations of results. In bulk materials, this gauge problem can be solved by using the same uniform k-grid which carries identical gauges for both GW-BSE and EPC calculations in the ExPC problem.[10] However, in 2D materials, very dense k-point sampling is needed to converge the exciton calculations, making the usage of a uniform k-grid across the whole BZ in both the GW-BSE and DFPT calculations computationally challenging. In monolayer WSe_2, we find that the k-grid density equivalent to 14,400 points in the BZ is necessary to capture the exciton energy and the exciton wave functions. To resolve this problem, we first use

https://doi.org/10.1021/acs.jpclett.4c01433
J. Phys. Chem. Lett. 2024, 15, 7584−7590

Downloaded from pubs.acs.org/jpcld/article-pdf/15/30/7584/3367608/jz4c01433.pdf by PEKING UNIV user on 04 November 2026

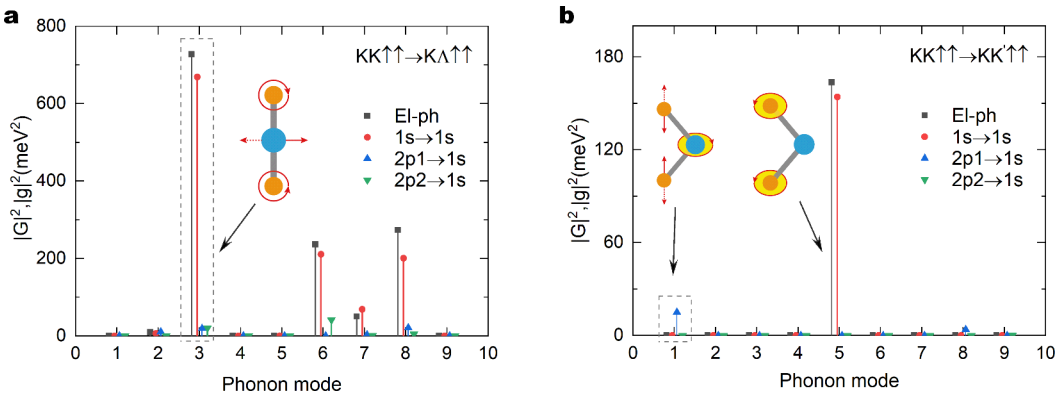

Figure 2. Modulus square of the ExPC matrix elements, $|G|^2$, for the scattering from three initial states, KK ↑↑ 1*s* (red circle), KK ↑↑ 2*p*1 (blue triangle), KK ↑↑ 2*p*2 (green inverted triangle) to two final states, KΛ ↑↑ 1*s* (a), KK′ ↑↑ 1*s* (b). The modulus squares of the EPC matrix elements ($|g|^2$) from K ↑ → Λ ↑ (a) and K ↑ → K′ ↑ (b) are also shown by black solid squares for comparison. Phonon modes 1 to 9 are numbered in ascending order in energy. In the side-view illustration of atomic vibrations (inset), an ellipse denotes the in-plane (of the 2D layer) rotation of the phonon eigenvector and a circle denotes the out-of-plane rotation of the phonon eigenvector.

the patch-sampling method in BSE calculations, which means that we do enhanced sampling at the *k* patches where the exciton envelope function is localized. The advantage of this technique is that a small number of sampled *k* points can have a very dense *k*-point sampling density. In monolayer WSe_2, 241 k points in the patch are used to reach the sampling density of 120 × 120 × 1 in the first BZ. Then, we choose the same gauge for the Bloch wave functions in BSE and EPC calculations. Since ExPC matrix element *G* itself is gauge-invariant, we can switch to any gauge for the envelope function and EPC matrix element to investigate ExPC. A physically motivated hydrogen gauge is applied, making the envelope function of the 1*s* exciton real.[35] After that, the EPC matrix element is rotated. This hydrogen gauge allows us to denote the exciton bands using the principal and the angular quantum numbers of 2D hydrogen atoms, and define a winding number of the EPC matrix elements. Other calculation details are included in Supporting Information.

Figure 1(a) schematically shows the phonon-mediated relaxation paths of the direct exciton in monolayer WSe_2. Possible initial states considered in our study are 1*s* and 2*p* direct excitons, denoted as KK ↑↑ 1*s* and KK ↑↑ 2*p*. Here we label the excitons by the valley-spin configuration of their constituent electron and hole, with that of the hole on the left. Due to the presence of 3-fold rotation symmetry and the absence of inversion symmetry, a KK ↑↑ 1*s* exciton can be resonantly excited by a circularly polarized photon.[36,37] Similarly, after absorbing two (or more) circularly polarized photons, a KK ↑↑ 2*p* exciton can be formed, which may relax into lower-energy and/or indirect excitons. Figure 1(c)-(e) show eigenvalues of the direct and indirect 1*s* and 2*p* excitons from GW-BSE calculations. The energy difference between the bright KK ↑↑ exciton and the dark KK ↑↓ one is attributed to the conduction band splitting, the exchange interaction, and the different effective mass for the two conduction bands around K valley. In our calculations, the energies of KΛ ↑↑ and KΛ′ ↑↓ 1*s* excitons are lower than KK ↑↑ and KK ↑↓ 1*s* excitons by 0.1−0.2 eV, which is slightly different from the approximate degeneracy found in a recent experiment.[26] This discrepancy arises from the choice of exchange-correlation functional and lattice constants used in the mean-field calculation (see Figure S3 in Supporting Information), and as we will show later, this minor difference does not affect the analysis of ExPC. Note that the two 2p states are degenerate in Figure 1(d)-(e) but not in Figure 1(c). This is caused by the Berry curvature effects on the relative motion of the electron−hole pair.[38,39]

To unveil the rules of exciton−phonon scattering and how they differ from electron−phonon scattering in conventional studies, we select three initial exciton states, i.e., KK ↑↑ 1*s*, 2*p*1 and 2*p*2, and two final exciton states, i.e., KΛ ↑↑ 1*s* and KK′ ↑↑ 1*s*, in the analysis. We focus on the ExPC matrix elements in eq 2, and extract the essential physics of scattering between initial and final exciton bands. For the electron−phonon scattering, we only consider the EPC matrix element for the intervalley scattering where the initial and final electrons are at the valley edges, respectively. This is usually adopted in conventional group theory studies of electron−phonon scattering. In other words, we compare the EPC matrix element at *K* point with the ExPC matrix element. In the following, it can be seen that the excitonic effects can involve a bunch of EPC matrix elements around *K* point, where distinct exciton−phonon selection rules can be developed with respect to the electron−phonon selection rule at *K* point. In calculations of the scattering time, we include the energy conservation relation in the exciton−phonon scattering events to account for the density-of-state effects. During the exciton−phonon scattering events of interest, while the electron is scattered to a different valley, the hole in monolayer WSe_2 resides in the same K valley. As a result, only the first term (electron−phonon scattering) of *G* in eq 2 can be nonzero.

At the EPC level, the matrix elements corresponding to intervalley scatterings of electrons from K to K′ or Λ show apparent phonon-mode dependence in Figure 2. This can be understood by group theory analysis (details in Sec. I of Supporting Information). The groups of wavevectors are C_{1h} and C_{3h} at Λ(Λ′) and K (K′), respectively, making the electron−phonon selection rules accessible by transforming the EPC matrix elements under an in-plane reflection $\hat{\sigma}_h$ and/or 3-fold rotation $\hat{C}_3$. For the K ↑ → Λ ↑ scattering, the allowed phonon modes, i.e. the second, third, sixth, seventh, and eighth modes in Figure 2(a), are symmetric under $\hat{\sigma}_h$. For K ↑ → K′ ↑, the allowed phonon modes need not only to be symmetric under $\hat{\sigma}_h$, but also to conserve the 3-fold pseudoangular momentum.[40] As a result, only the fifth mode is allowed as shown in Figure 2(b).

Downloaded from pubs.acs.org/jpcld/article-pdf/15/30/7584/3367608/jz4c01433.pdf by PEKING UNIV user on 04 November 2026

https://doi.org/10.1021/acs.jpclett.4c01433
J. Phys. Chem. Lett. 2024, 15, 7584−7590

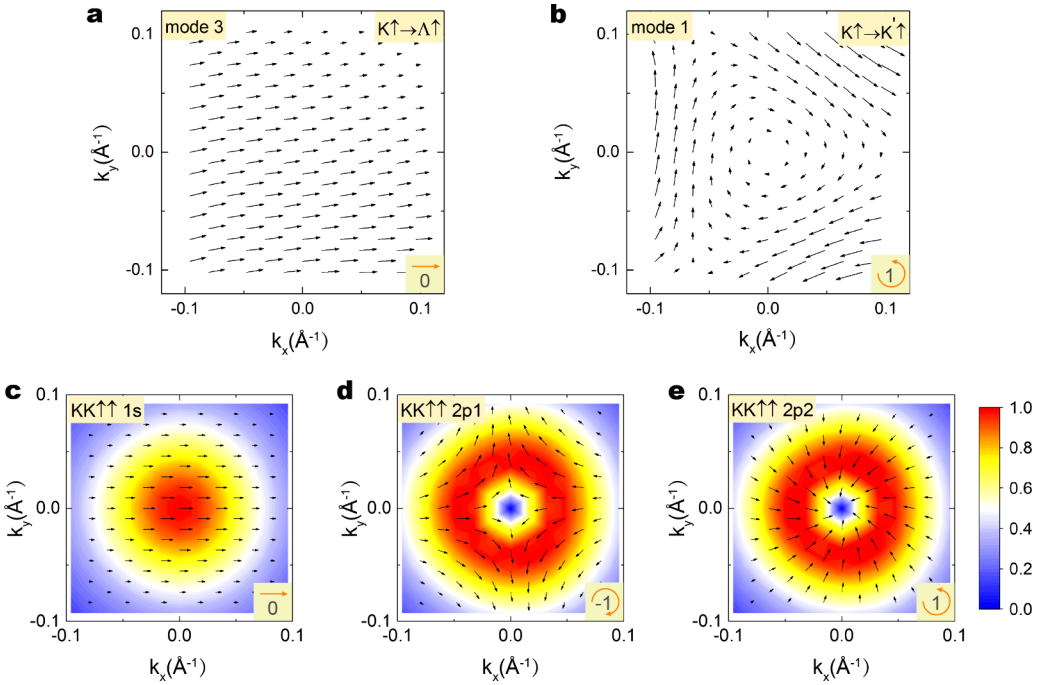

Figure 3. Selection rules of ExPC. (a–b) The distribution of the calculated EPC matrix elements in the BZ for the electron–phonon scattering of K ↑ → Λ ↑ and K ↑ → K′ ↑. (c–e) The distribution of exciton envelope functions of 1*s*, 2*p*1 and 2*p*2 states of the KK ↑↑ excitons in the BZ. The envelope functions are normalized by their largest values. The color and length (direction) of an arrow denote(s) the magnitude (phase) of the envelope function and EPC matrix element. a and b are used to calculate the exciton–phonon scattering from three KK ↑↑ states to two final states, i.e. KΛ ↑↑ 1*s* and KK′ ↑↑ 1*s*, respectively. The origin is at the extreme *k*-point K. The orange arrow in the corner denotes the topology of the distribution of envelope functions and EPC matrix elements around the extreme *k*-point. The numbers in the corner denote the exciton angular quantum number or winding number of EPC matrix elements.

At the ExPC level, however, these selection rules are significantly changed. The ExPC matrix elements exhibit distinct features from those of EPC due to the influence of the exciton envelope function that carries angular momentum (eq 2). First, excitons with different principal and angular quantum numbers interact differently with a given phonon mode. This is a feature completely missing in the analysis of the EPC matrix elements. For the third mode in Figure 2(a), although the ExPC scattering strength of 1*s* → 1*s* is similar to that of the EPC scattering, the strengths of 2*p*1 → 1*s* and 2*p*2 → 1*s* decrease sharply. More interestingly, conventional group theory analysis of the EPC matrix element shows that the first mode in Figure 2(b) cannot contribute to the scattering. At the exciton–phonon level, however, the strength of 2*p*1 → 1*s* is greatly enhanced, exceeding the strength of the 1*s* → 1*s* process. Similar distinctions between the ExPC and EPC matrix elements have also been found for the scattering into KΛ′ exciton (Figure S7 in Supporting Information).

These unusual exciton–phonon scattering patterns motivate us to explore the selection rules generic to the exciton–phonon scattering problems in 2D Wannier exciton systems. Since the envelope function of the first few low-energy Wannier exciton is highly localized in *k*-space, in eq 2, the summation over *k*-points can be performed in the vicinity of the respective band extreme of the hole at $\boldsymbol{k}_0$, or the electron at $\boldsymbol{k}_0 + \boldsymbol{Q}$. The envelope function of the exciton Rydberg states can be written as $A^S_{\nu\boldsymbol{k},c\boldsymbol{k}+\boldsymbol{Q}} \approx R_{nl}(|\boldsymbol{k}'|)e^{il\theta_{\boldsymbol{k}'}}$, where $\boldsymbol{k}' = \boldsymbol{k} - \boldsymbol{k}_0$. $\theta_{\boldsymbol{k}'}$ denotes the azimuthal angle of $\boldsymbol{k}'$.[41] *n* and *l* are the principal and angular quantum numbers of exciton *S*. The radial part, $R_{nl}(|\boldsymbol{k}'|)$, is real while the angular part, $e^{il\theta_{\boldsymbol{k}'}}$, rotates in the complex plane for nonzero *l*. For a particular phonon mode ν that scatters electrons between two nondegenerate bands, the continuity of *k*-resolved EPC matrix elements allows us to map them to a vector field tangential to the BZ, and use the winding number to character the phase of the EPC matrix elements. For example, to scatter an electron near the conduction band minimum at $\boldsymbol{k}_0 + \boldsymbol{Q}$, the EPC matrix elements can be written as $g_{c'c}(\boldsymbol{k}+\boldsymbol{Q},\boldsymbol{q}\nu) \approx T_{c'c,m}(|\boldsymbol{k}'|,\boldsymbol{q}\nu)e^{im\theta_{\boldsymbol{k}'}}$, where *m* is the winding number. In the case of exciton–phonon scattering that changes the momenta of bound electrons (e.g., monolayer WSe_2), the ExPC matrix element (eq 2) can be rewritten as

$$G_{n'l',nl}(\boldsymbol{Q},\boldsymbol{q}\nu) \approx \sum_{\boldsymbol{k}'} \tilde{R}_{n'l'}(|\boldsymbol{k}'|)R_{nl}(|\boldsymbol{k}'|)T_{c'c,m}(|\boldsymbol{k}'|,\boldsymbol{q}\nu) \times e^{i(l-l'+m)\theta_{\boldsymbol{k}'}} \quad (3)$$

Equation 3 involves the dominant contribution from the first term in eq 2. For simplicity, we include one valence and one conduction band. The generalization to hole-phonon scattering and multiband cases is straightforward. From eq 3, the winding number of EPC matrix elements should contribute to the change of exciton angular quantum numbers for the allowed scattering, giving rise to the selection rule,

$$l - l' + m = 0 \quad (4)$$

Equation 4 shows that ExPC is fundamentally different from EPC, and gives unexpected phonon-mediated scattering between excitons of different angular momentum if the EPC winding number *m* is nonzero.

The selection rules in eq 4 can be used to understand the first-principles results in Figure 2. Figure 3(c)-(e) show normalized envelope functions of the 1*s*, 2*p*1, and 2*p*2 states of the KK ↑↑ exciton in the BZ. They are very localized with the

https://doi.org/10.1021/acs.jpclett.4c01433
J. Phys. Chem. Lett. 2024, 15, 7584–7590

Downloaded from pubs.acs.org/jpclcd/article-pdf/15/30/7584/3367608/jz4c01433.pdf by PEKING UNIV user on 04 November 2026

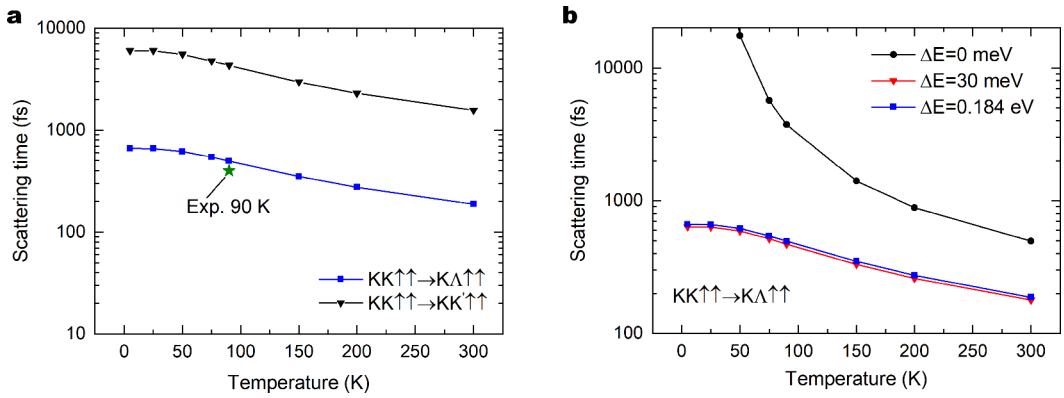

Figure 4. Intervalley exciton scattering times. (a) Calculated T-dependent scattering times of KK 1s excitons for two channels. The experimental value from ref 26 at 90 K is marked by a star. (b)The T-dependent scattering times for different energy differences between initial and final states. In a, the energy difference ΔE used is 0.18 eV.

extension radius of ∼0.1 Å^{-1}, highlighting the importance of dense k-sampling in GW-BSE calculations. The quantum phase of the envelope functions allows us to identify that 2p1 and 2p2 states have angular quantum numbers l of −1 and 1, respectively. The two final 1s states, KΛ ↑↑ and KK′ ↑↑, both have l' = 0. Figure 3(a)-(b) show the k-resolved EPC matrix elements between different electron valleys, for processes highlighted in Figure 2. The K → Λ (ν = 3) and K → K' (ν = 1) EPC matrix elements have winding numbers m of 0 and 1, respectively. In Figure 3(b), the first phonon mode is forbidden for the K ↑ → K′ ↑ electron−phonon scattering. However, this scattering becomes allowed at neighboring k-points of K due to symmetry reduction. Geometrically, K becomes a critical point in the vector-field representation of EPC matrix elements in Figure 3(b), leading to a winding number of 1. According to eq 4, this winding number 1 could compensate the angular quantum number −1 of the KK ↑↑ 2p1 exciton, and allow the first phonon mode to scatter KK ↑↑ 2p1 → KK′ ↑↑ 1s (Figure 2(b)). In Figure 3(a), however, since Λ has the same symmetry as that of its neighboring k-points, the K ↑ → Λ ↑ (ν = 3) EPC matrix elements are nearly the same. As a result, the third mode could contribute to the scattering KK ↑↑ 1s → KΛ ↑↑ 1s rather than KΛ ↑↑ 2p1 or KΛ ↑↑ 2p2. Note that for the scattering from the KK exciton to the KK′ exciton, there exists the conservation of 3-fold rotation symmetry. One can obtain the eigenvalues of 3-fold rotational operation $\hat{C}_3$ on the exciton wave function and the phonon eigenvector, respectively. Then the pseudoangular momentum of the phonon mode contributes to the change of excitonic $\hat{C}_3$ eigenvalues from the initial to final exciton state for allowed ExPC. In eq 4, however, we use the conservation between the winding number of the EPC matrix element and the angular quantum numbers of the exciton envelope function. For KK → KK′, these two kinds of theoretical analysis are essentially the same. But, eq 4 is suitable for more general exciton−phonon scattering, like KK → KΛ, where the final exciton state does not have 3-fold rotation symmetry.

Finally, we apply our first-principles algorithm and selection rules to study the intervalley relaxation pathways of KK ↑↑ 1s excitons. In the low exciton density limit which corresponds to linear optical response, the exciton−phonon scattering rate can be written as[28]

$$\Gamma_{S\mathbf{Q}} = \frac{2\pi}{\hbar}\frac{1}{N_q}\sum_{S'\boldsymbol{q}\nu}|G_{S'S}(\mathbf{Q},\boldsymbol{q}\nu)|^2[(n_{\boldsymbol{q}\nu}+1)\delta(\Omega_{S\mathbf{Q}}-\Omega_{S'\mathbf{Q}+\boldsymbol{q}}-\hbar\omega_{\boldsymbol{q}\nu}) + n_{\boldsymbol{q}\nu}\delta(\Omega_{S\mathbf{Q}}-\Omega_{S'\mathbf{Q}+\boldsymbol{q}}+\hbar\omega_{\boldsymbol{q}\nu})] \quad (5)$$

where $n_{\boldsymbol{q}\nu}$ is the Bose distribution function of phonons. Phonon modes satisfying the energy conservation relation are sampled in the phonon BZ, where a 30 × 30 × 1 q-grid is used and interpolated into 240 × 240 × 1. Here, we are mostly interested in one-phonon-assisted exciton intervalley scattering. Also, we only include the spin-conserving scattering processes in the summation over final states. Spin-non-conserving scattering is generally slower, and is calculated in a separate work.[12] We note that our method relies on the harmonic approximation of phonons. However, the anharmonic effects are insignificant for phonon dispersions of bulk WSe_2.[42] We thus estimate that anharmonic effects do not contribute significantly to the exciton−phonon scattering time. Quantitative calculations of anharmonic effects are beyond the scope of this work and may be described using *ab initio* nonadiabatic molecular dynamics simulations.[14,43] Details of calculations and other approximations (i.e., effective mass description of exciton energy and wave function) are included in Supporting Information.

Figure 4(a) shows the temperature (T)-dependent scattering times of the two dominant processes, i.e., KK ↑↑ → KΛ ↑↑ and KK ↑↑ → KK′ ↑↑. The T dependence is mainly caused by the phonon occupation number. At ∼ 90 K, the calculated scattering time of KK ↑↑ → KΛ ↑↓ is ∼500 fs, agreeing well with the measured value ∼400 fs. In Figure 4(b), we plot the T-dependent scattering times for the different energy differences. In the degenerate case, we notice a divergent scattering time at low Ts since only the phonon-absorption scattering process can take place and the phonon occupation number is near zero. However, if KK ↑↑ 1s is higher than KΛ ↑↑ 1s by 30 meV (within the experimental spectral resolution), the scattering time significantly decreases and becomes almost the same as ΔE = 0.18 eV, the value we used in Figure 4(a).

This insensitivity to the energy difference is understandable by a density-of-states argument. The largest phonon frequency with the quasi-momentum around $\boldsymbol{q} = \boldsymbol{\Lambda} - \boldsymbol{K}$ is ∼35 meV. When the energy difference is in the range from 30 to 184 meV, on one hand, the number of final states that can be scattered into by phonon is similar; on the other hand, the ExPC strength weakly depends on the phonon quasi-momentum which connects the initial and final exciton states.

Downloaded from pubs.acs.org/jpcld/article-pdf/15/30/7584/3367608/jz4c01433.pdf by PEKING UNIV user on 04 November 2026

https://doi.org/10.1021/acs.jpclett.4c01433
J. Phys. Chem. Lett. 2024, 15, 7584−7590

As a result, according to the eq 5, the scattering time for KK ↑↑ → KΛ ↑↑ nearly does not change when the energy difference increases from 30 to 184 meV. Another factor that may affect the scattering time is the exciton exchange interaction. At a finite temperature, the excited KK (K′K′) 1*s* excitons could have a nonzero center-of-mass momentum after thermalization.[26] This can change the energy conservation condition in eq 5, if the exchange interactions are incorporated, which would give rise to linear exciton dispersions.[44−46] However, we believe that the change of scattering time would be small, for the same reason as the insensitivity discussed above. We conclude that the exciton intervalley scattering observed in ref.[26] mainly arises from phonon-mediated KK ↑↑ → KΛ ↑↑ process.

We developed an accurate and efficient first-principles method for calculating ExPC in 2D semiconductors. For 2D Wannier excitons, we found distinct ExPC selection rules compared with conventional EPC selection rules. The derived ExPC selection rules require that the winding number of EPC matrix elements should match the change of exciton angular quantum number to make ExPC allowed. These numerical results shed light on the microscopic mechanism of exciton relaxations in recent experiments.[26] Further studies that include spin-flip scattering channels may also unveil rich patterns in the EPC matrix element and unexpected scattering pathways. Considering the recent surge of research about excitonic properties in layered materials, especially TMD, we believe the selection rules discovered and the computational method developed here can stimulate both theoretical and experimental studies of exciton−phonon interactions in more 2D semiconductors.

■ ASSOCIATED CONTENT

Supporting Information

The Supporting Information is available free of charge at https://pubs.acs.org/doi/10.1021/acs.jpclett.4c01433.

Details of GW-BSE calculations, electron−phonon scattering, exciton−phonon scattering, and exciton scattering times (PDF)

Transparent Peer Review report available (PDF)

■ AUTHOR INFORMATION

Corresponding Authors

En-Ge Wang − *International Center for Quantum Materials and School of Physics, Peking University, Beijing 100871, People's Republic of China; School of Physics, Liaoning University, Shenyang 110036, People's Republic of China*; Email: egwang@pku.edu.cn

Xin-Zheng Li − *Interdisciplinary Institute of Light-Element Quantum Materials and Research Center for Light-Element Advanced Materials, State Key Laboratory for Artificial Microstructure and Mesoscopic Physics, Frontier Science Center for Nano-optoelectronics and School of Physics, Peking University, Beijing 100871, People's Republic of China*; orcid.org/0000-0003-0316-4257; Email: xzli@pku.edu.cn

Ting Cao − *Department of Materials Science and Engineering, University of Washington, Seattle, Washington 98195, United States*; orcid.org/0000-0003-1300-6084; Email: tingcao@uw.edu

Authors

Xiao-Wei Zhang − *International Center for Quantum Materials and School of Physics, Peking University, Beijing 100871, People's Republic of China*; orcid.org/0000-0002-0158-9385

Kaichen Xie − *Department of Materials Science and Engineering, University of Washington, Seattle, Washington 98195, United States*; orcid.org/0000-0001-8479-8301

Complete contact information is available at: https://pubs.acs.org/10.1021/acs.jpclett.4c01433

Notes

The authors declare no competing financial interest.

■ ACKNOWLEDGMENTS

X.-W.Z., E.-G.W., and X.-Z.L. are supported by the National Science Foundation of China under Grant Nos. 11934003 and 12234001, the National Basic Research Programs of China under Grant Nos. 2021YFA1400503 and 2022YFA1403500, the Beijing Natural Science Foundation under Grant No. Z200004, and the Strategic Priority Research Program of the Chinese Academy of Sciences under Grant No. XDB33010400. K.X. and T.C. are supported by NSF through the University of Washington Materials Research Science and Engineering Center Grant No. DMR-1719797. The computational resources were supported by the high-performance computing platform of Peking University, China.

■ REFERENCES

(1) Sjakste, J.; Vast, N.; Tyuterev, V. Ab initio Method for Calculating Electron-Phonon Scattering Times in Semiconductors: Application to GaAs and GaP. *Phys. Rev. Lett.* **2007**, *99*, 236405.

(2) Giustino, F. Electron-phonon interactions from first principles. *Rev. Mod. Phys.* **2017**, *89*, 015003.

(3) Song, X.; Hu, J.; Zeng, H. Two-dimensional semiconductors: recent progress and future perspectives. *J. Mater. Chem. C* **2013**, *1*, 2952−2969.

(4) Xiao, J.; Zhao, M.; Wang, Y.; Zhang, X. Excitons in atomically thin 2D semiconductors and their applications. *Nanophotonics* **2017**, *6*, 1309−1328.

(5) Manzeli, S.; Ovchinnikov, D.; Pasquier, D.; Yazyev, O. V.; Kis, A. 2D transition metal dichalcogenides. *Nat. Rev. Mater.* **2017**, *2*, 17033.

(6) Wang, G.; Chernikov, A.; Glazov, M. M.; Heinz, T. F.; Marie, X.; Amand, T.; Urbaszek, B. Colloquium: Excitons in atomically thin transition metal dichalcogenides. *Rev. Mod. Phys.* **2018**, *90*, 021001.

(7) Xu, X.; Yao, W.; Xiao, D.; Heinz, T. F. Spin and pseudospins in layered transition metal dichalcogenides. *Nat. Phys.* **2014**, *10*, 343−350.

(8) Mak, K. F.; Xiao, D.; Shan, J. Light−valley interactions in 2D semiconductors. *Nat. Photonics* **2018**, *12*, 451−460.

(9) Cardona, M.; Peter, Y. Y. *Fundamentals of Semiconductors*; Springer: Berlin, 2005.

(10) Chen, H.-Y.; Sangalli, D.; Bernardi, M. Exciton-phonon interaction and relaxation times from first principles. *Phys. Rev. Lett.* **2020**, *125*, 107401.

(11) Reichardt, S.; Wirtz, L. Nonadiabatic exciton-phonon coupling in Raman spectroscopy of layered materials. *Sci. Adv.* **2020**, *6*, No. eabb5915.

(12) Zhang, X.-W.; Cao, T. Ab initio calculations of spin-nonconserving exciton−phonon scattering in monolayer transition metal dichalcogenides. *J. Phys.: Condens. Matter* **2022**, *34*, 264002.

(13) Chan, Y.-h.; Haber, J. B.; Naik, M. H.; Neaton, J. B.; Qiu, D. Y.; da Jornada, F. H.; Louie, S. G. Exciton Lifetime and Optical Line Width Profile via Exciton−Phonon Interactions: Theory and First-Principles Calculations for Monolayer MoS_2. *Nano Lett.* **2023**, *23*, 3971−3977.

Downloaded from pubs.acs.org/jpclcd/article-pdf/15/30/7584/3367608/jz4c01433.pdf by PEKING UNIV user on 04 November 2026

(14) Jiang, X.; Zheng, Q.; Lan, Z.; Saidi, W. A.; Ren, X.; Zhao, J. Real-time GW-BSE investigations on spin-valley exciton dynamics in monolayer transition metal dichalcogenide. *Sci. Adv.* **2021**, *7*, No. eabf3759.
(15) Liu, J.; Zhang, X.; Lu, G. Excitonic effect drives ultrafast dynamics in van der Waals heterostructures. *Nano Lett.* **2020**, *20*, 4631−4637.
(16) Liu, J.; Lu, G.; Zhang, X. Exciton dispersion and exciton−phonon interaction in solids by time-dependent density functional theory. *J. Chem. Phys.* **2023**, *158*, 044116.
(17) Amit, T.; Refaely-Abramson, S. Ultrafast exciton decomposition in transition metal dichalcogenide heterostructures. *Phys. Rev. Mater.* **2023**, *108*, L220305.
(18) Huang, T. A.; Zacharias, M.; Lewis, D. K.; Giustino, F.; Sharifzadeh, S. Exciton−phonon interactions in monolayer germanium selenide from first principles. *J. Phys. Chem. Lett.* **2021**, *12*, 3802−3808.
(19) Antonius, G.; Louie, S. G. Theory of exciton-phonon coupling. *Phys. Rev. B* **2022**, *105*, 085111.
(20) Lechifflart, P.; Paleari, F.; Sangalli, D.; Attaccalite, C. First-principles study of luminescence in hexagonal boron nitride single layer: Exciton-phonon coupling and the role of substrate. *Phys. Rev. Mater.* **2023**, *7*, 024006.
(21) Cohen, G.; Haber, J. B.; Neaton, J. B.; Qiu, D. Y.; Refaely-Abramson, S. Phonon-driven femtosecond dynamics of excitons in crystalline pentacene from first principles. *Phys. Rev. Lett.* **2024**, *132*, 126902.
(22) He, K.; Kumar, N.; Zhao, L.; Wang, Z.; Mak, K. F.; Zhao, H.; Shan, J. Tightly bound excitons in monolayer WSe_2. *Phys. Rev. Lett.* **2014**, *113*, 026803.
(23) Zhang, C.; Chen, Y.; Johnson, A.; Li, M.-Y.; Li, L.-J.; Mende, P. C.; Feenstra, R. M.; Shih, C.-K. Probing critical point energies of transition metal dichalcogenides: surprising indirect gap of single layer WSe_2. *Nano Lett.* **2015**, *15*, 6494−6500.
(24) Hsu, W.-T.; Lu, L.-S.; Wang, D.; Huang, J.-K.; Li, M.-Y.; Chang, T.-R.; Chou, Y.-C.; Juang, Z.-Y.; Jeng, H.-T.; Li, L.-J.; Chang, W.-H. Evidence of indirect gap in monolayer WSe_2. *Nat. Commun.* **2017**, *8*, 929.
(25) Elliott, J. D.; Xu, Z.; Umari, P.; Jayaswal, G.; Chen, M.; Zhang, X.; Martucci, A.; Marsili, M.; Merano, M. Surface susceptibility and conductivity of MoS_2 and WSe_2 monolayers: A first-principles and ellipsometry characterization. *Phys. Rev. B* **2020**, *101*, 045414.
(26) Madéo, J.; Man, M. K.; Sahoo, C.; Campbell, M.; Pareek, V.; Wong, E. L.; Al-Mahboob, A.; Chan, N. S.; Karmakar, A.; Mariserla, B. M. K.; Li, X.; Heinz, T. F.; Cao, T.; Dani, K. M. Directly visualizing the momentum-forbidden dark excitons and their dynamics in atomically thin semiconductors. *Science* **2020**, *370*, 1199−1204.
(27) Toyozawa, Y. Theory of line-shapes of the exciton absorption bands. *Prog. Theor. Phys.* **1958**, *20*, 53−81.
(28) Knox, R. S. *Theory of excitons*; Academic Press, 1963.
(29) Strinati, G. Application of the Green's functions method to the study of the optical properties of semiconductors. *Riv. Nuovo Cimento* **1988**, *11*, 1−86.
(30) Rohlfing, M.; Louie, S. G. Electron-hole excitations and optical spectra from first principles. *Phys. Rev. B* **2000**, *62*, 4927.
(31) Qiu, D. Y.; da Jornada, F. H.; Louie, S. G. Optical spectrum of MoS_2: many-body effects and diversity of exciton states. *Phys. Rev. Lett.* **2013**, *111*, 216805.
(32) Qiu, D. Y.; da Jornada, F. H.; Louie, S. G. Screening and many-body effects in two-dimensional crystals: Monolayer MoS_2. *Phys. Rev. B* **2016**, *93*, 235435.
(33) Deslippe, J.; Samsonidze, G.; Strubbe, D. A.; Jain, M.; Cohen, M. L.; Louie, S. G. BerkeleyGW: A massively parallel computer package for the calculation of the quasiparticle and optical properties of materials and nanostructures. *Comput. Phys. Commun.* **2012**, *183*, 1269−1289.
(34) Giannozzi, P.; et al. QUANTUM ESPRESSO: a modular and open-source software project for quantum simulations of materials. *J. Phys.: Condens. Matter* **2009**, *21*, 395502.
(35) Cao, T.; Wu, M.; Louie, S. G. Unifying optical selection rules for excitons in two dimensions: Band topology and winding numbers. *Phys. Rev. Lett.* **2018**, *120*, 087402.
(36) Cao, T.; Wang, G.; Han, W.; Ye, H.; Zhu, C.; Shi, J.; Niu, Q.; Tan, P.; Wang, E.; Liu, B.; et al. Valley-selective circular dichroism of monolayer molybdenum disulphide. *Nat. Commun.* **2012**, *3*, 887.
(37) Xiao, D.; Liu, G.-B.; Feng, W.; Xu, X.; Yao, W. Coupled spin and valley physics in monolayers of MoS_2 and other group-VI dichalcogenides. *Phys. Rev. Lett.* **2012**, *108*, 196802.
(38) Srivastava, A.; Imamoğlu, A. Signatures of Bloch-band geometry on excitons: nonhydrogenic spectra in transition-metal dichalcogenides. *Phys. Rev. Lett.* **2015**, *115*, 166802.
(39) Zhou, J.; Shan, W.-Y.; Yao, W.; Xiao, D. Berry phase modification to the energy spectrum of excitons. *Phys. Rev. Lett.* **2015**, *115*, 166803.
(40) Zhang, L.; Niu, Q. Chiral phonons at high-symmetry points in monolayer hexagonal lattices. *Phys. Rev. Lett.* **2015**, *115*, 115502.
(41) Cohen, M. L.; Louie, S. G. *Fundamentals of Condensed Matter Physics*; Cambridge University Press, 2016.
(42) Gupta, M. K.; Kumar, S.; Mittal, R.; Mishra, S. K.; Rols, S.; Delaire, O.; Thamizhavel, A.; Sastry, P.; Chaplot, S. L. Distinct anharmonic characteristics of phonon-driven lattice thermal conductivity and thermal expansion in bulk $MoSe_2$ and WSe_2. *J. Mater. Chem. A* **2023**, *11*, 21864−21873.
(43) Zheng, Z.; Shi, Y.; Zhou, J.-J.; Prezhdo, O. V.; Zheng, Q.; Zhao, J. Ab initio real-time quantum dynamics of charge carriers in momentum space. *Nat. Comput. Sci.* **2023**, *3*, 532−541.
(44) Qiu, D. Y.; Cao, T.; Louie, S. G. Nonanalyticity, valley quantum phases, and lightlike exciton dispersion in monolayer transition metal dichalcogenides: Theory and first-principles calculations. *Phys. Rev. Lett.* **2015**, *115*, 176801.
(45) Yu, H.; Cui, X.; Xu, X.; Yao, W. Valley excitons in two-dimensional semiconductors. *Natl. Sci. Rev.* **2015**, *2*, 57−70.
(46) Wu, F.; Qu, F.; MacDonald, A. H. Exciton band structure of monolayer MoS_2. *Phys. Rev. B* **2015**, *91*, 075310.

Downloaded from pubs.acs.org/jpclcd/article-pdf/15/30/7584/3367608/jz4c01433.pdf by PEKING UNIV user on 04 November 2026

https://doi.org/10.1021/acs.jpclett.4c01433
J. Phys. Chem. Lett. 2024, 15, 7584−7590